Using geochemistry and environmental tracers to study shallow unconfined aquifer recharge and mineralization processes in the Yinchuan Plain, arid Northwest China

YongFeng Gong, Xin Liu, Bin Ma, PengFei Qi and Yan Li

ABSTRACT

Irrigation water extracted from the Yellow River plays a key role in water resource management in the Yinchuan Plain (YCP), arid Northwest China. Investigating the soluble matters (ion and gas) of groundwater provides information to explain the unconfined shallow aquifer recharge and groundwater mineralization processes after long-term flood irrigation activity. Environmental tracing with the elements, ^{2}H, ^{18}O, ^{3}H, and CFCs, combining geochemistry using major ions and selected trace elements, was conducted for 43 water samples from September to October 2019 in the YCP. Evaporite and silicate weathering dominate the shallow unconfined groundwater geochemical compositions. Water–rock interactions control the mineralization characteristics regularly along the groundwater flow paths from the southwest toward the northeast. Stable isotopes suggest that Yellow River water and precipitation in winter and/or from Helan Mountainous area are the main recharge sources. The shallow unconfined aquifer mixed young (post-1940) and old (pre-1940) water with young water ratios from 53.1 to 73.5% inferred from the CFC concentrations and ^{3}H activities. Water reinfiltrations extracted from the Yellow River and from the old groundwater are confirmed. Lateral flow recharge for the shallow unconfined aquifer is less indistinctive than that from the water re-infiltration in the plain areas.

Key words | arid area, geochemistry and isotope, groundwater recharge, mineralization processes, Yinchuan Plain

HIGHLIGHTS

- Groundwater lateral flow recharge is substantially less than irrigation re-infiltration in the shallow unconfined aquifer.
- Irrigation water extracted from the Yellow River and groundwater have different recharge ratios for the shallow unconfined aquifer.
- Evaporite and silicate weathering dominate the shallow unconfined groundwater geochemical compositions.

YongFeng Gong
Bin Ma (corresponding author)
PengFei Qi
School of Environmental Studies,
China University of Geosciences,
Wuhan 430074,
China
E-mail: *bma@cug.edu.cn*

YongFeng Gong
Ningxia Institute of Land and Resources Survey and Monitoring,
Yinchuan 750002,
China

Xin Liu
Bureau of Hydrology, Changjiang Water Resources Commission,
Wuhan 430010,
China

Yan Li
Ningxia Institute of Hydrology and Water Resources Monitoring and Early Warning,
Yinchuan 750002,
China

doi: 10.2166/nh.2021.143

INTRODUCTION

Groundwater is an essential but invisible resource and even acts as a unique water source in arid areas. Ascertaining groundwater sources usually proves elusory for people due to their complexity and invisibility. Investigating hydrogeological and geochemical processes such as aquifer recharge, groundwater mixing, and mineralization processes is an efficient way for ensuring sustainability, protection, and proper management of water resources in arid areas in the face of both anthropogenic and climate-driven changes (Edmunds *et al.* 2006; Han *et al.* 2011; Ma *et al.* 2018). The geochemistry in arid areas is generally controlled by (1) groundwater recharge source and mixing characteristic, (2) mineralization processes, (3) residence time, and (4) evaporation along the groundwater flow path within the aquifer (Ma *et al.* 2013). Geochemistry and environmental tracers (e.g. ^{2}H, ^{18}O, ^{3}H, ^{14}C, and CFCs) are being increasingly incorporated into studies to contribute to the understanding of groundwater recharge sources, mixing characteristics and mineralization processes (Zhu *et al.* 2007; Huang *et al.* 2017; Fackrell *et al.* 2020).

The stable isotopes ^{2}H and ^{18}O are widely used by hydrogeologists in tracing the water cycle because of their distinctive characteristics, such as conservativeness and, as molecules of water, being naturally supplied by precipitation. They are often used as natural tracers in subsurface water flow paths in arid areas due to their phase variable features when evaporation, condensation, and sublimation occur. Studies on investigating groundwater recharge sources, water mixing and flow paths, groundwater salinization, and moisture cycle have been widely undertaken based on the stable isotope fractional mechanisms (Huang & Pang 2012; Kong & Pang 2016; Binet *et al.* 2017; Ma *et al.* 2017). Another molecule of water is tritium (^{3}H), which is radioactive with a half-life of 12.32 years, and is a powerful tracer to study groundwater recharge years and recharge sources (Tadros *et al.* 2014; Ma *et al.* 2019). ^{3}H is more widely used in the Northern Hemisphere due to its much higher activity caused by synthetic rather than natural conditions. The continual atmospheric thermonuclear tests in the Northern Hemisphere during the 1950s and 1960s have abundantly generated ^{3}H in the atmosphere, supplying us artificial tracers to study modern water recharge and water mixing features. Nowadays, rainfall ^{3}H activities are still affected by the tail end of the bomb pulse in the Northern Hemisphere, which is particularly seen in the arid northwest of China due to both the continental effect (Tadros *et al.* 2014) and the superimposition over China of the atmospheric nuclear tests from 1964 to 1974. Hence, a comprehensive use of the water isotopes (^{2}H, ^{18}O, and ^{3}H) provides virtual information for aquifer recharge and groundwater flow characteristics.

The synthetic chlorofluorocarbons (CFCs, e.g. CFC-11, CFC-12, and CFC-113) were first detected in the atmosphere in the 1940s. CFCs have relatively long transit times (44, 180, and 85 years for CFC-11, CFC-12, and CFC-113, respectively) than ^{3}H in the atmosphere, which allows their uniform atmospheric distributions over large areas, but there is 1–2 years of lag time for the Southern Hemisphere than for the Northern Hemisphere (Darling *et al.* 2012; Cartwright *et al.* 2017; Cook *et al.* 2017). Though the atmospheric CFC concentrations have declined since 1994 to date (different CFCs peaked at different times), there is a possibility for some ambiguity in regard to the CFC ratio plot (Darling *et al.* 2012). The different atmospheric CFC ratios that exist, that is those of today and those before the 1990s make investigating groundwater recharge years and mixing ratios by CFCs possible. Consequently, CFCs have been commonly viewed as alternatives to ^{3}H for estimating recharge years in groundwater with the decline in bomb-pulse ^{3}H activities (Qin *et al.* 2011; Cook *et al.* 2017). What should be noticed is the industrial contamination during both the groundwater recharge process and water sampling (Han *et al.* 2007; Qin 2007; Mahlknecht *et al.* 2017). The entrapped excess air makes the use of CFCs difficult to study the water cycle. The other adverse factors for using CFCs are degradation in anaerobic groundwater (Cook & Solomon 1995; Plummer *et al.* 2006; Horneman *et al.* 2008) in the confined aquifers and/or sorption in the soil.

Agricultural reclamation in the Yinchuan Plain (YCP) can be dated back to nearly 2000 years ago. Irrigation

water extracted from the Yellow River has long played an important role in maintaining the balance of groundwater resource as irrigation water re-infiltration into the aquifer is enormous, especially into the unconfined aquifer in the plain areas. Irrigation re-infiltration from canal systems constitutes 83% of the total groundwater recharge (Wang *et al.* 2004). Previous studies in the YCP have concluded that Yellow River water plays an important role in the shallow aquifer recharge based on isotopic data analyses (Su & Lin 2004; Fan 2018). Excessive groundwater exploitation and Yellow River irrigation recharge have changed the quality of the shallow aquifer groundwater critically in recent decades (Yang 2018).

The YCP is located in the arid Northwest China and is far from the industrialized cities, such as Beijing, Shanghai, and Guangzhou, and, thus, ^{3}H and CFCs are supposedly good tracers for investigating the shallow unconfined aquifer recharge. Hence, the aim of this study is to investigate the shallow unconfined aquifer recharge, groundwater mixing characteristics, and mineralization processes in the YCP after long-term irrigation activity by using geochemistry and environmental tracers.

STUDY AREA AND GEOLOGICAL SETTING

The YCP (Figure 1) is located in the north of the Ningxia Hui Autonomous Region and in the middle and upper reaches of the Yellow River. The southern border is Qingtongxia and is located northward to Shizuishan, and the western border is Helan Mountain and is located eastward to the western margin of the Ordos Plain. It is 165 km long from south to north and 42–60 km wide from west to east with a total area of 7,790 km^2. The YCP has a typical continental arid climate with an annual average temperature of 8.92 °C. January has the lowest average temperature of −7.73 °C, and the extreme minimum temperature is −30.6 °C. The highest average temperature is in July with 23.63 °C, and the extreme maximum temperature is 41.4 °C. The annual average precipitation is 186.7 mm, of which 68.1% occurs from June to September. The annual potential evaporation is 1,838.44 mm, 93.2% of which occurs from April to September. The annual average humidity is 55%.

The altitudes in the plain area vary from 1,100 to 1,200 m, where in the Helan Mountain, they vary from 1,500 to 3,200 m to the summit of 3,500 m. The plain area is consistent with the piedmont plain, alluvial–proluvial plain, and lacustrine plain with slopes of 10–30, 5, and 0.2–1.8‰, respectively. The lacustrine plain has witnessed cultivation for nearly 2000 years, which is still an important production area for agriculture, forestry, animal husbandry, and fisheries.

Figure 2 displays the strata structures of the YCP, which consist of pre-tertiary (AnR) and tertiary (N) in the marginal plain (the strata basements of the YCP) and the quaternary system. Quaternary strata with a thickness of >1,600 m distributes along the line of the Pingluo–Yaofu–Yinchuan areas. The Lower Pleistocene (Q_1), Middle Pleistocene (Q_2), Upper Pleistocene (Q_3), and Holocene (Q_4) are demarcated in Figure 2. The lithology explanations are also given. Sandy gravel is mainly distributed in the piedmont plain, and the lithology becomes fine in the central and eastern plains and consists of fine sand, clayey sand, and sandy sand.

The porous aquifers are divided into two types, which are the single unconfined aquifer and multilayer aquifers. The single unconfined aquifer distributes along the Helan Mountain in the west and south of YCP, and the thickness varies from 10 to 300 m with sandy gravel and some pebbles. The water depth varies from 0.5 to 4.0 m, and the water abundance varies from 2,000 to 5,000 m^3/d. Detailed data are given in Figure 1. The multilayer aquifers consist of an unconfined aquifer, the first confined aquifer, and the second confined aquifer from top to bottom within 250 m under the surface. What can be noticed is that the three aquifers are obstructed by a discrete aquitard, which indicates that there are hydraulic connections among each other.

The unconfined aquifer has a thickness of 20–60 m and distributes in the alluvial–proluvial plain and lacustrine plain. Figure 2 shows that the water abundance decreases to 1,000–3,000 m^3/d in the central area and to <1,000 m^3/d in the north of the YCP. The first confined aquifer top depths vary from 25 to 60 m and bottom depth varies from 140 to 160 m with a total thickness of 120 m. The second confined aquifer has a total thickness of 60–125 m and its bottom depth reaches 240–260 m. Overall, the aquifer thickness decreases from the central area to the western and eastern margins of the YCP.

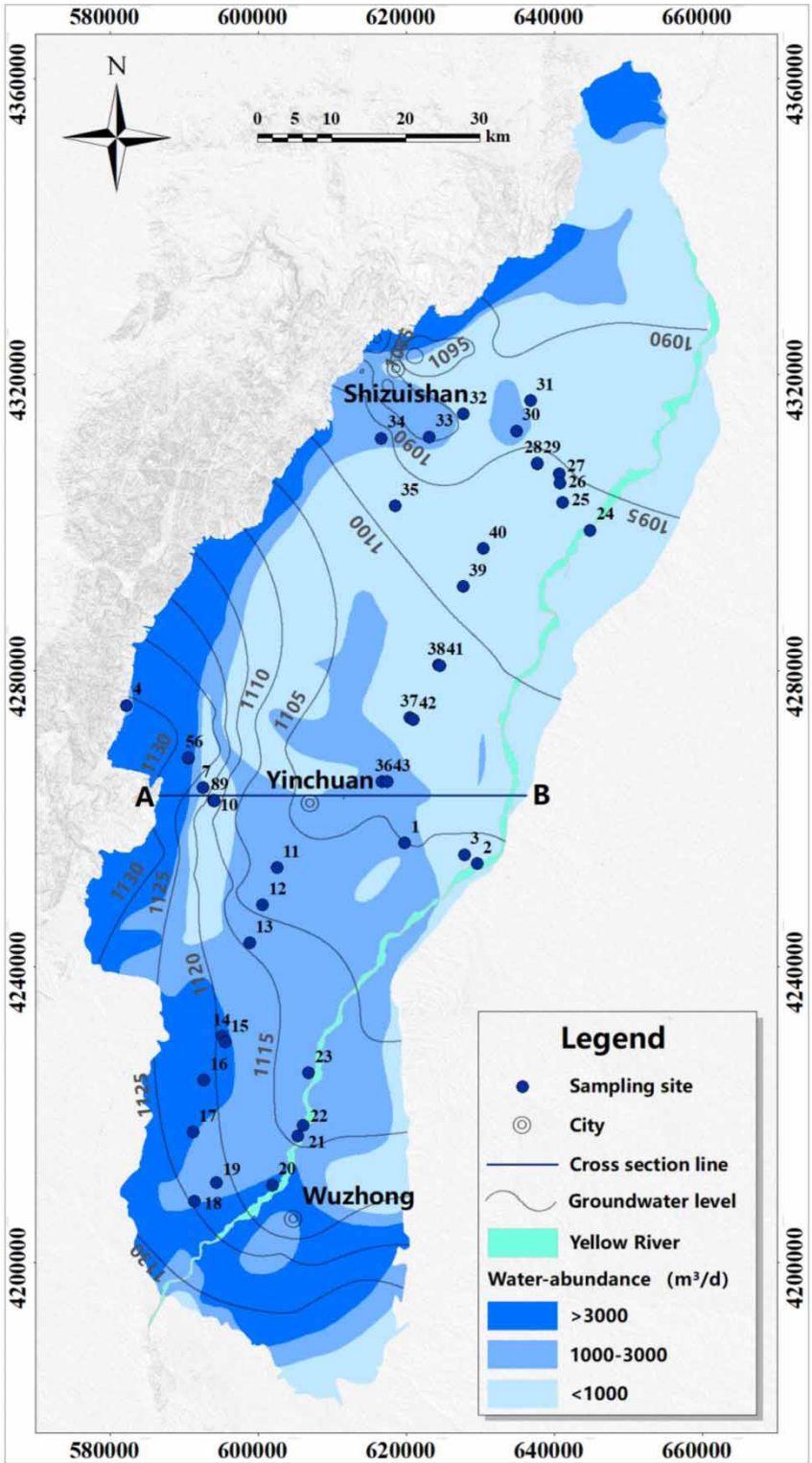

Figure 1 | The geographic map of the Yinchuan Plain with the groundwater level and sampling sites for a shallow unconfined aquifer.

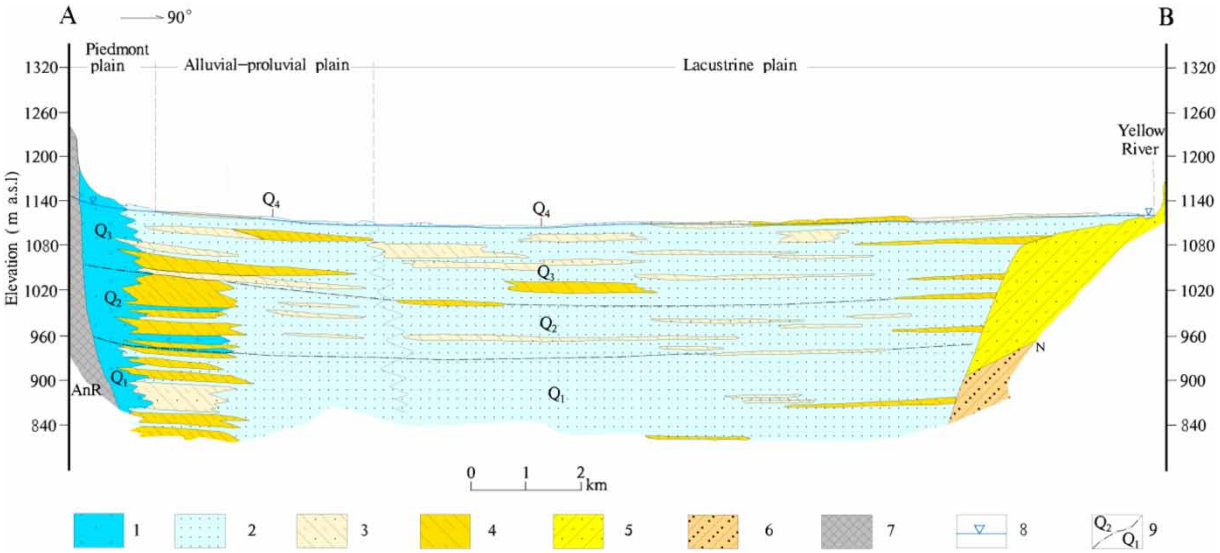

Figure 2 | Hydrogeological cross section of the Yinchuan Plain for the A–B line shown in Figure 1. Explanations are as follows: 1, Sandy gravel; 2, Fine sand; 3, Clayey sand; 4, Sandy clay; 5, Argillaceous sandstone; 6, Sandstone; 7, Pre-tertiary; 8, Water table; 9, Geological boundary.

SAMPLING AND METHODS

Field sampling

A total of 43 water samples were taken in the YCP, including three Yellow River water samples (collected along the river flow direction), one spring sample, and 39 groundwater samples. Groundwater was pumped from agricultural and domestic wells (Figure 1 and Table 1), in which the wells were pumped for a minimum of 10 min prior to sampling.

Water temperature (T), electrical conductivity (EC), and pH values were measured in the field using calibrated Hach (HQ40d) conductivity and pH meters (Table 1), which had been calibrated before use. Bicarbonate was determined by titration with 0.05 N HCl on-site. Samples to be analyzed for geochemistry and environmental isotopes (δ^2H, $\delta^{18}O$, and ^3H) were filtered on-site through 0.45 μm millipore syringe filters and stored in pre-cleaned polypropylene bottles at 4 °C until analysis. Water samples for ^3H analysis were collected and stored in 500 mL airtight polypropylene bottles. For cation analysis, the samples were acidified to pH <2 with ultrapure HNO_3.

CFCs are dissolved gases, and, thus, extreme precautions are needed to be taken to avoid contamination from equipment such as pumps and tubing for CFC samples (Han *et al.* 2012; Cook *et al.* 2017). After purging the wells, the water samples were collected directly from the borehole using a copper tube sampling pipe for CFC analysis. One end of the pipe was connected to the well casing, and the other end was placed at the bottom of a 120 mL borosilicate glass bottle, inside a 2,000 mL beaker. The well water was allowed to flow through the tubing for 10 min, leading to a thorough flushing of the tubing. The bottle was submerged, filled, and capped underwater till no bubbles appeared in the bottle, following the protocols described by Ma *et al.* (2019). In this study, six bottles were collected at each well and three of them were analyzed. A total of eight wells were collected for CFC (CFC-11, CFC-12, and CFC-113) analysis.

Laboratory analyses

The calculations of the stable isotopic values (δ^2H and $\delta^{18}O$) and the geochemical calculations for water were performed at the Institute of Geological Survey, China University of Geosciences (Wuhan). δ^2H and $\delta^{18}O$ analyses were done using a Liquid Water Isotopic Analyzer (LGR, IWA-45EP, USA). The δ^2H and $\delta^{18}O$ values (Table 1) were presented in δ notation in ‰ with respect to the Vienna Standard Mean Ocean Water (VSMOW), with an analytical precision of 0.5‰ vs. VSMOW for δ^2H and of 0.1‰ for $\delta^{18}O$. Cations were analyzed using an inductively coupled plasma atomic emission spectrometer (ICP-AES) (IRIS Intrepid II XSP, Thermo Elemental).

Table 1 | Geochemistry, stable isotopes, CFC concentrations, and tritium (^{3}H) activity of surface water and groundwater in the Yinchuan Plain

Sample ID	Well depth (m)	pH	T (°C)	EC (μS/cm)	K (mg/L)	Na (mg/L)	Ca (mg/L)	Mg (mg/L)	Sr (mg/L)	Si (mg/L)	Cl (mg/L)	SO_4 (mg/L)	HCO_3 (mg/L)	TDS (mg/L)	δ^2H (‰)	$\delta^{18}O$ (‰)	^3H (TU)
Yellow River water																	
YC-2		7.78	16.7	632	1.8	52.1	64.0	24.0	0.792	3.18	48.7	103.0	219.1	403.4	−67.2	−9.8	
YC-22		7.82	18.7	612	2.1	41.0	58.8	22.4	0.847	3.12	37.7	88.8	223.9	367.8	−66.3	−9.8	
YC-24		7.81	17	639	1.8	41.0	52.8	20.0	0.716	2.59	44.0	94.2	224.1	374.8	−67.2	−9.9	
Spring																	
YC-4		7.82	16.5	390	1.5	19.7	51.4	7.6	0.306	7.62	16.8	36.2	220.7	245.3	−77.3	−11.3	
Groundwater																	
YC-1	20	7.29	16	2,230	3.2	191.0	246.0	131.0	2.82	6.12	160.0	437.0	405.0	1,818.7	−68.7	−9.6	10.48
YC-3	25	7.53	14.5	1,539	2.2	228.0	100.0	45.7	1.6	6.38	143.0	240.0	468.0	993.3	−67.7	−9.1	9.91
YC-5	5	7.50	22.3	2,130	3.7	304.0	98.8	92.0	0.898	7.28	224.0	372.0	518.5	1,432.8	−77.7	−11.2	
YC-6	18	7.41	14.7	2,240	4.1	288.0	116.0	112.0	1.1	7.34	253.0	431.0	468.8	1,512.5	−77.4	−11.2	3.14
YC-7	25	7.63	14.6	1,665	3.5	282.0	87.4	58.3	0.828	7.46	171.0	311.0	399.9	1,122.5	−72.7	−10.1	
YC-8	18	7.73	16.3	1,150	2.7	96.1	77.0	57.9	0.909	7.35	105.0	166.0	310.4	703.8	−71.1	−9.9	
YC-9	12	7.77	15.2	1,073	2.3	82.3	66.6	49.9	0.779	6.46	93.6	161.0	279.5	638.6	−70.9	−9.8	
YC-10	26	7.43	15.8	767	2.3	57.5	61.3	42.2	0.757	6.84	55.2	83.9	299.0	452.2	−78.5	−11.1	7.88
YC-11	25	7.60	14.8	892	2.2	89.3	63.7	23.6	0.679	5.57	82.0	150.0	201.1	521.3	−55.2	−6.5	7.49
YC-12	20	7.84	15	918	2.2	73.0	67.1	46.3	2.44	7.5	74.0	135.0	208.1	566.0	−68.6	−9.4	
YC-13	30	7.68	15.3	1,222	2.3	95.4	144.0	47.6	2.08	7.93	77.2	159.0	352.9	802.0	−65.8	−9.2	
YC-14	20	7.43	15.3	1,826	3.6	256.0	71.5	101.0	2.1	6.6	165.0	267.0	580.5	1,168.9	−69.6	−9.4	
YC-15	25	7.57	13.3	1,228	2.1	84.5	136.0	43.9	2	5.57	94.4	167.0	459.1	757.8	−68.7	−9.4	
YC-16	15	7.56	14.7	1,364	4.5	95.0	98.6	74.2	2.47	5.68	91.5	192.0	466.8	818.7	−68.2	−9.6	
YC-17	14	7.53	15.7	1,308	3.3	92.7	100.0	70.8	2.2	7.63	93.0	198.0	495.9	806.0	−69.1	−9.8	
YC-18	9	7.63	16.4	1,205	3.2	73.8	121.0	41.6	1.84	5.03	71.6	163.0	405.4	735.4	−69.2	−10.2	
YC-19		7.66	18.5	1,007	2.3	72.4	102.0	45.1	1.46	6.26	67.7	138.0	375.5	616.0	−72.6	−9.8	
YC-20	8	7.24	17.7	2,040	7.8	155.0	244.0	90.3	3.39	7.27	195.0	285.0	755.6	1,364.6	−67.9	−9.5	
YC-21	13	7.58	16.2	1,193	2.8	82.7	94.9	43.6	1.7	6.27	95.3	138.0	447.5	681.3	−62.8	−8.0	
YC-23	15	7.57	13.6	1,956	1.3	176.0	177.0	105.0	2.72	4.79	163.0	325.0	459.3	1,332.9	−65.3	−9.2	
YC-25	12	7.66	13.1	1,328	1.8	94.3	95.9	34.0	1.64	5.56	143.0	181.0	377.9	739.3	−75.9	−11.0	
YC-26		7.72	16.9	1,425	1.5	191.7	88.6	67.2	2.58	5.54	227.0	164.0	322.7	903.2	−86.7	−12.6	
YC-27	12	7.47	14	2,050	2.5	261.0	176.0	94.0	1.59	6.53	225.0	380.5	543.7	1,411.1	−74.7	−10.8	
YC-28	12	7.68	12.1	923	1.1	70.1	49.5	47.9	1.25	5.72	75.6	92.8	358.0	516.3	−73.5	−10.1	

(*continued*)

Table 1 | continued

Sample ID	Well depth (m)	pH	*T* (°C)	EC (μS/cm)	K (mg/L)	Na (mg/L)	Ca (mg/L)	Mg (mg/L)	Sr (mg/L)	Si (mg/L)	Cl (mg/L)	SO_4 (mg/L)	HCO_3 (mg/L)	TDS (mg/L)	δ^2H (‰)	$\delta^{18}O$ (‰)	^3H (TU)
YC-29		7.74	13.2	873	1.0	89.2	43.6	35.0	1.09	5.75	80.3	91.5	299.2	490.5	−73.5	−10.0	
YC-30	15	7.30	12.7	3,580	6.5	590.0	148.0	163.0	3.11	4.97	435.0	791.0	704.0	2,511.1	−70.6	−9.8	
YC-31	15	7.69	14	1,008	2.2	77.0	98.3	35.6	2.35	5.8	74.0	138.0	352.7	601.7	−68.7	−9.6	
YC-32	13	7.70	14.7	4,930	3.6	945.9	235.8	200.7	4.16	4.36	1,180.6	880.7	340.8	3617.9	−85.7	−11.4	
YC-33	22	7.62	14.7	6,000	2.0	953.0	458.0	98.1	4.2	6.22	1,247.0	1,253.0	407.8	4,215.3	−60.8	−7.4	
YC-34	42	7.84	14.7	480	1.3	35.8	49.9	16.9	1.01	6.35	27.6	42.0	208.1	277.8	−75.7	−10.3	
YC-35	15	7.81	15.4	391	0.5	45.4	32.5	10.8	0.639	6.37	11.1	6.3	238.0	225.9	−91.7	−12.6	
YC-36	12	7.42	14.7	2,050	2.8	275.0	178.0	81.2	1.68	5.07	165.0	379.0	594.7	1,426.8	−66.6	−9.1	
YC-37	15	7.45	13.5	1,627	5.8	163.0	112.0	108.0	1.92	5.8	132.0	271.0	565.2	1,074.7	−72.6	−10.1	
YC-38	15	7.47	13.3	2,160	4.7	233.0	176.0	111.0	2.78	4.17	181.0	505.0	547.6	1,484.8	−69.8	−9.6	
YC-39	18	7.63	16.9	1,357	7.1	150.0	112.0	57.6	1.27	4.96	113.0	230.0	405.8	872.9	−70.6	−9.7	
YC-40	20	7.34	14.2	2,420	2.4	385.8	148.3	128.6	2.6	5.33	330.7	400.2	670.7	1,731.6	−54.2	−6.5	
YC-41	32	7.58	11.2	2.024	2.59	206	148	112	2.41	6.06	221.4	283.7	521.1	1,240.6	−77.1	−10.8	9.91
YC-42	50	7.56	12.1	1.629	1.27	175	87.5	88.4	1.86	5.79	132.9	226.3	573.0	1,005.4	−78.8	−11.1	8.63
YC-43	10	7.36	13	2.21	2.9	246	136	137	2.66	4.77	185.8	413.2	556.5	1,498.1	−71.1	−9.9	8.03

Anions were analyzed on filtered unacidified samples using an ion chromatograph (IC) (Metrohm 761 Compact IC). Analytical errors were inferred from the mass balance between cations and anions (with HCO_3) and were within ±10%.

The ^3H activities of groundwater were measured using a liquid scintillation spectrometer (1220 Quantulus ultra-low-level counters, PerkinElmer, Waltham, MA, USA) at the Experimental Center of School of Environmental Studies, China University of Geosciences (Wuhan). Water samples for ^3H were distilled and electrolytically enriched prior to being analyzed. Detailed procedures were followed by Morgenstern & Taylor (2009). ^3H activities were expressed as tritium unit (TU), with 1 TU corresponding to a $^3H/^1H$ ratio of 1×10^{-18}. The achieved precision for ^3H was ±0.2 TU.

The CFC concentrations were analyzed within 2 months of sample collection at the Groundwater Dating Laboratory of the Institute of Geology and Geophysics, Chinese Academy of Sciences (IGG-CAS), using a purge-and-trap gas chromatography procedure with an Electron Capture Detector, which has been reported by Qin *et al.* (2011). The procedures were followed by Oster *et al.* (1996). The detection limit for each CFC is about 0.01 pmol/L of water, with the error being less than ±5%. The measured results are shown in Table 2.

CFCs estimating groundwater recharge year

A knowledge of the history of the atmospheric CFC concentrations is first required for groundwater recharge time dating. The YCP locates in the Northwest China and is far from the industrial city with low population density, and thus, we would hypothesize that there is no clear difference in the atmospheric CFC concentrations between North America and the YCP. To evaluate CFC ages, the time-series trend of Northern Hemisphere atmospheric mixing ratio between 1940 and 2017 was adopted in this study.

Measured CFC concentrations (in pmol/L) can be interpreted in terms of the partial pressures of CFCs (in pptv) in solubility equilibrium with the water sample based on Henry's Law solubility (Table 2). The concrete computational process was the one followed by Plummer *et al.* (2006). In the arid northwest China, the local shallow groundwater temperature was found more suitable than the annual mean surface air temperature to be estimated for the recharge temperature (Qin *et al.* 2011), as the local low precipitation usually cannot reach the groundwater. Previous studies have demonstrated that irrigation infiltration and lateral flow recharge from the piedmont area were much more abundant than the vertical recharge from the precipitation in the YCP. In this study, the measured groundwater temperature varied from 11.2 to 22.3 °C from each well (Table 1) as the recharge temperature was used to estimate the groundwater recharge year. The water recharge year was then determined by comparing the calculated partial pressures of CFC concentrations (in pptv) in solubility equilibrium with the water samples with historical CFC concentrations in the air based on the hypothesis of piston flow.

Table 2 | Calculated results for CFC atmospheric partial pressure (pptv), fraction of post-1940 water, and young precipitation recharge year

	Measured CFCs (pmol/L)			Atmospheric partial pressure (pptv)					Recharge year (calendar year)		
Sample ID	CFC-11	CFC-12	CFC-113	CFC-11	CFC-12	CFC-113	Mixing post-1940 water in decimal year (F12/F113)	Fraction of post-1940 water (BM, %)	CFC-11	CFC-12	CFC-113
YC-1	0.33	1.34	0.09	25.31	382.69	23.04	1986	53.1	1965	1985	1980
YC-3	0.33	0.82	0.11	23.28	217.23	25.71			1965	1975	1981
YC-6	2.21	2.56	0.38	158.31	687.69	90.28			1979		
YC-10	0.61	1.64	0.14	45.70	458.24	34.99			1969	1988	1984
YC-11	4.48	1.91	0.25	319.13	510.15	59.10				1992	1988
YC-41	0.32	0.85	0.09	19.01	193.09	17.41	1983	54.7	1964	1974	1979
YC-42	0.52	0.89	0.12	32.36	210.77	24.44	1986	53.9	1966	1975	1981
YC-43	0.51	0.99	0.1	33.45	245.81	21.56	1982	73.5	1967	1976	1980

BM, binary mixing, assuming a mixture of CFC-free water (pre-1940) with young water (post 1940).

RESULTS AND DISCUSSION

Mechanisms controlling mineralization processes

Geochemical sources of groundwater

Ion ratios and their relationship between each other provide essential information for identifying geochemical sources in groundwater. It is seen from Figure 3 that the water samples are along the mixing trend among the silicate and evaporite end members obtained by Gaillardet *et al.* (1999). Spring water is located in the silicate end member (Figure 3(a)), which indicates different ion sources and different recharge flow pathways from the Yellow River water and groundwater samples. Spring water was collected in the piedmont area and was recharged from the mountainous groundwater lateral flow during which the rock was found to be different from that in the plain area. As weathering of different parent rocks (e.g. carbonate, silicate, and evaporite) yields different combinations of dissolved cations and anions to solution, the groundwater in the plain area shows a relatively wide range and falls on a line, indicating mixing between different rocks. Meanwhile, all of the water samples tend to fall within the evaporite and silicate end members and are even far from the carbonate weathering domain, showing very low values in the HCO_3/Na and Mg/Na vs. Ca/Na plot (Figure 3). This indicates that weathering of evaporite and silicate has an influence on the geochemical compositions of groundwater in the YCP. Yellow River water samples overlap with some of the groundwater ones, indicating that either they have the same original mineral rocks or they are derived from the same recharge sources.

Water–rock interactions

The geochemical compositions of water within an aquifer are usually influenced by many factors, including lithology, dissolution and precipitation, ion exchange, mixing characteristic, and residence time. Water–rock interactions show a comprehensive reflection of many factors mentioned above. It is seen in Figure 4(a) that some ions and ion ratios are compared with each other to highlight the different mechanisms contributing to water–rock interactions in the YCP. Chloride as an inert element is widely used for denoting inputs and providing information on water–rock interactions in groundwater. Figure 4(a) shows a linear relationship between Na and Cl, likely indicating that some of the Na originated from halite dissolution. The variable molar Na/Cl ratios (calculated from Table 1) suggest that large water–rock interactions occur. Furthermore, any increase in molar Na/Cl ratios above 1.0 (Appelo & Postma 2005) would suggest some reaction of silicate minerals or cation exchange releasing Na at the expense of

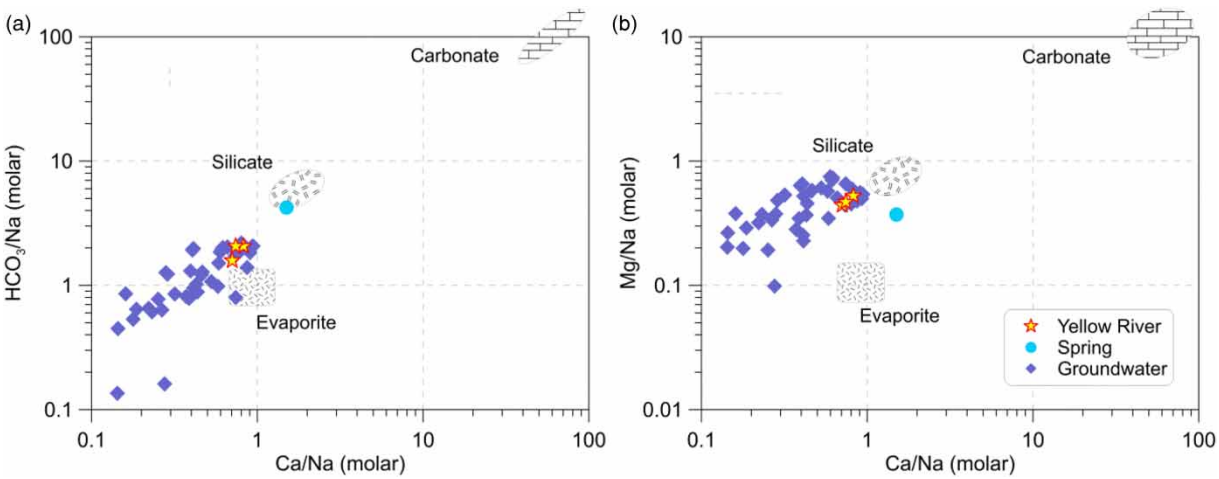

Figure 3 | Plots of (a) HCO_3/Na vs. Ca/Na and (b) Mg/Na vs. Ca/Na in water samples in the YCP. The correlations are shown in a log–log space. The carbonate, silicate, and evaporite end members obtained from Gaillardet *et al.* (1999) are presented.

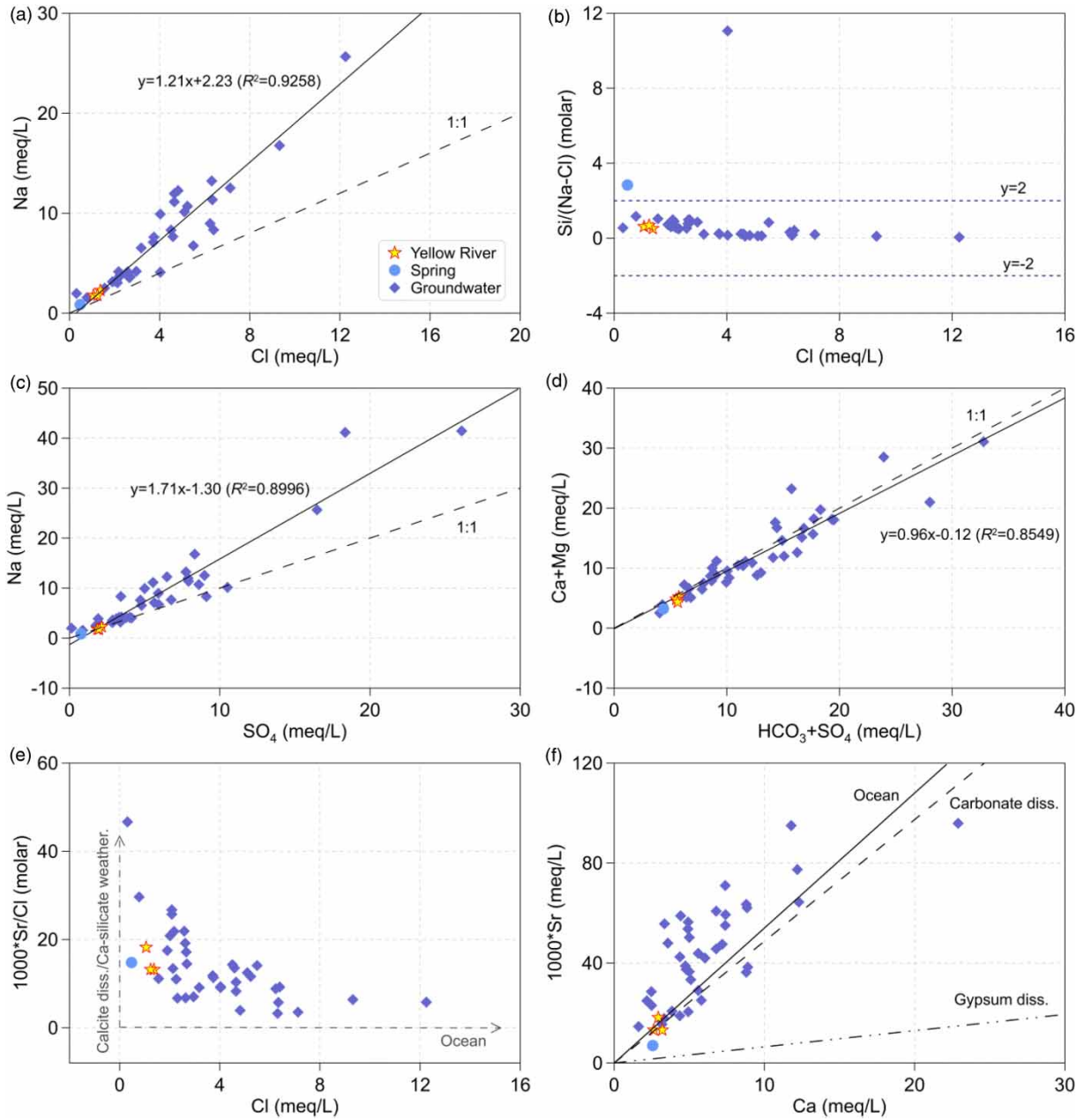

Figure 4 | Plots of the relationship between various ions and their ratios of water in the YCP. Oceanic ratios and carbonate and gypsum dissolution trends in plot (f) are from Cartwright *et al.* (2007).The solid lines represent the linear relationship of the results in (a), (c) and (d). The molar ratios of ±2 of Si/(Na-Cl) in (b) and the trends for Calcite dissolution and/or Ca-silicate weathering and in Ocean in (e) are shown in dashed lines.

some other cation. Meanwhile, the linear Na and Cl are at variance with the 1:1 ratio, which makes us infer that the excess Na might have originated from silicate and other evaporates (inferred from Figure 3). Previous studies in the arid areas of Northwest China have demonstrated that feldspar weathering would contribute to the high Na/Cl ratios in the groundwater (Ma *et al.* 2013, 2018). The very low molar K/Na ratios (mean 0.0210 calculated from Table 1) led us to conclude that albeit over K-feldspar weathering would supply extra Na composition in the YCP groundwater. Therefore, the following chemical equation for albite weathering, which releases Na, partially

explains the high molar Na/Cl ratios of the groundwater:

$$2NaAlSi_3O_8 + 9H_2O + 2H_2CO_3 = Al_2Si_2(OH)_4 + 2Na + 2HCO_3 + 4H_4SiO_4 \quad (1)$$

It is seen from Figure 4(b) that the molar ratios of Si/(Na–Cl) for groundwater (except for groundwater No. 25) and Yellow River water totally show low values with a mean value of 0.47, which is largely smaller than 2. When considering only the albite weathering followed by Equation (1), it would result in a molar Si/(Na–Cl) ratio of ±2 for the groundwater. Therefore, we could make a hypothesis that the excess Na probably did not originate solely from silicate weathering, as no silicate weathering reaction could explain such a low ratio (Stallard & Edmond 1987). Figure 4(c) shows a good linear relationship between Na and SO_4 ($R^2 = 0.8996$, meq./L), indicating that sodium sulfate (Na_2SO_4) dissolution is likely be another potential source of excess Na. Figure 4(d) also displays a good linear relationship for Ca + Mg and $HCO_3 + SO_4$ for all of the water samples and generally distributes along the 1:1 stoichiometry ratios, which indicate that Ca, Mg, HCO_3, and SO_4 are most probably derived from a dissolution of calcite, dolomite, and gypsum. Alternatively, the small variance from the 1:1 stoichiometry ratio when $HCO_3 + SO_4$ was high would make us infer that there are other sources from HCO_3 and SO_4. It is seen in Equation (1) that this reaction would generate HCO_3 and, thus, account for the high HCO_3 contents. Considering the charge balance between anions and cations, the excess negative charge of HCO_3 and SO_4 must be balanced by Na, which suggests that sodium and bicarbonate can be trolled by the dissolution of trona ($Na_2CO_3{\cdot}NaHCO_3{\cdot}2H_2O$) to some extent. Trona dissolution has been widely confirmed in the groundwater in the arid Northwest China (Ma *et al.* 2013, 2018).

It is seen in Figure 4(e) that the molar Sr/Cl ratios vary from 0.00032 to 0.00142 in the study area and are overall higher than that in the ocean (Cartwright *et al.* 2007), indicating that the additional sources of Sr, except for the ocean, would be attributed to the water–rock interactions. Calcite dissolution and/or Ca-silicate (for example, anorthite) weathering might account for the high Sr/Cl ratios. Furthermore, Figure 4(f) displays three end members that explain different contributions to the Ca and Sr ratios. It is seen that all of the water samples deviate from the gypsum dissolution end member but distribute close to the ocean and carbonate dissolution end members. Therefore, Figure 4(e) and 4(f) imply comprehensively that Sr typically results from significant carbonate dissolution, though some Sr-bearing evaporites such as gypsum and celestite can significantly elevate the concentrations of Sr in groundwater. Meanwhile, Figure 4(f) shows relatively high molar 1,000*Sr/Ca ratios for the groundwater (varying from 4.1 to 16.6 with a mean value of 7.9), which could be ascribed to calcite precipitate during the water–rock interaction processes.

To examine which minerals would dissolve or precipitate in the aquifer, the saturation indices (SIs) with respect to halite, dolomite, calcite, gypsum, and anhydrite of all water samples in the YCP were calculated using PHREEQC 2 (Parkhurst & Appelo 1999). Figure 5(a) and 5(d) display logarithmic trends between SIs (halite, gypsum, and anhydrite) and ion concentrations, respectively (Cl and SO_4, in meq/L), in which the negative SIs indicate an undersaturated state and these minerals in sediments can easily enter the groundwater. In contrast, in Figure 5(b) and 5(c), it is seen that dolomite and calcite SIs are both positive values, indicating an oversaturated state with respect to calcite and dolomite mineral phases for all of the waters. This phenomenon also supports the hypothesis inferred from Figure 4(f) that the high molar Sr/Ca ratios in the water samples are due to calcite precipitation.

The mineral SI implies important information concerning groundwater flow pathways and residence time, which have been proved in previous studies in the arid areas (Edmunds *et al.* 2006; Ma *et al.* 2018). Synthesizing the sampling site and groundwater levels (shown in Figure 1), we can infer that mineral saturation increases gradually along the flow paths from Wuzhong (southern and piedmont area of the YCP) and Yinchuan (west of the YCP) to Shizuishan and Yellow River circum, which is common in the regional groundwater flow paths from the recharge zone toward the groundwater discharge zone.

Shallow unconfined aquifer recharge and mixing characteristics

Groundwater recharge sources based on δ^2H, $\delta^{18}O$ and CFCs

As water molecule components, the stable isotopes (^2H and ^{18}O) are widely used to account for soil water infiltration,

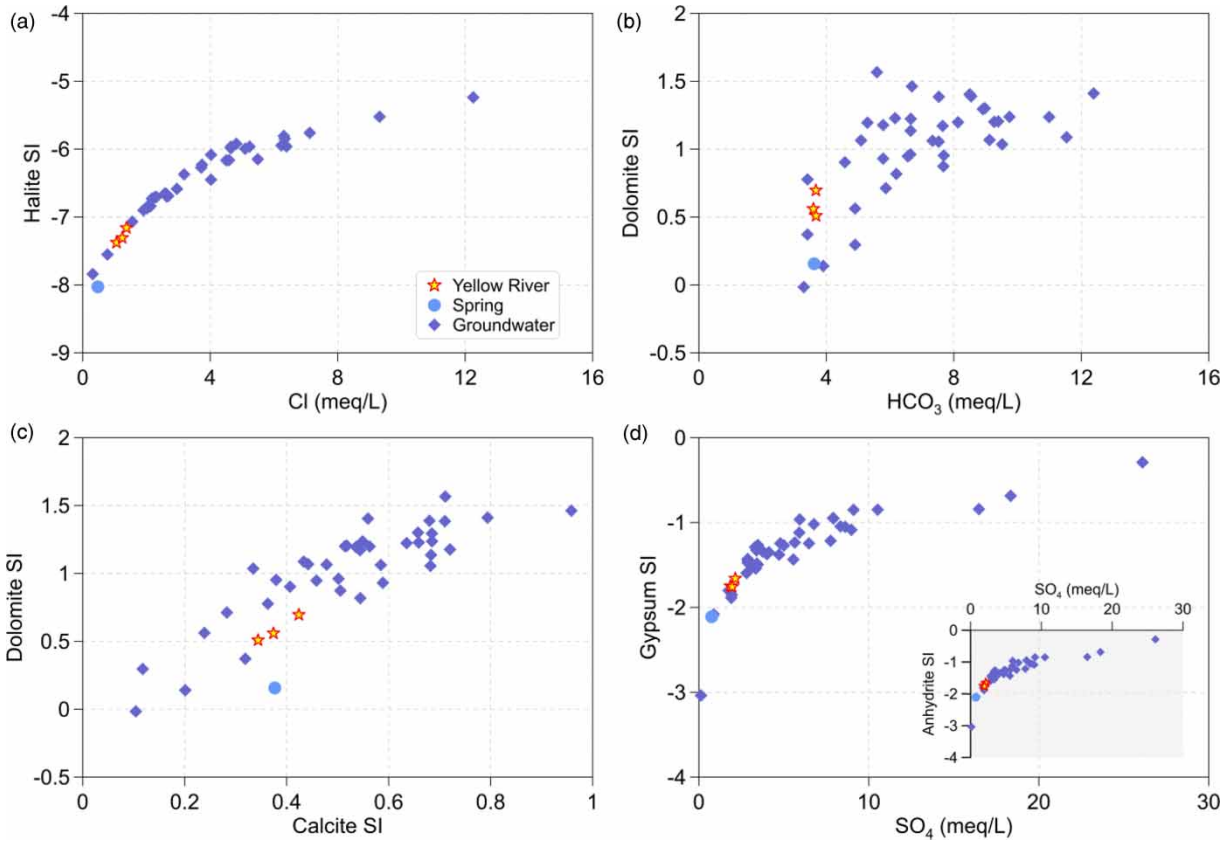

Figure 5 | Plots showing relationships of SIs for (a) halite vs. Cl, (b) dolomite vs. HCO_3, (c) dolomite SI vs. calcite SI, and (d) gypsum and anhydrite vs. SO_4 of water samples in the study area.

water mixing, aquifer recharge, and groundwater flow processes. Their isotope proportions vary immediately when physical and chemical conditions change, for example temperature, air humidity, wind speed, when contacting with surrounding rock, and so on. Modern precipitation is generally more enriched in ^{2}H and ^{18}O than paleo-meteoric precipitation due to the higher temperatures in modern-day climates. Furthermore, precipitation in the winter and/or with higher elevation generally occurs with more depleted isotopes, and, thus, the groundwater recharge sources from different elevations and from different seasons could be identified. Based on the above considerations, the relationship between $\delta^{2}H$ and $\delta^{18}O$ from the precipitation collected in different months, the annual precipitation mean values, and the water samples collected in the study area are displayed in Figure 6.

It is seen in Figure 6(a) that all of the water samples in the YCP are plotted along the Global Meteoric Water Line (GMWL, Craig 1961) and the Local Meteoric Water Line (LMWL, the data are from rainfall in the Yinchuan station of IAEA networks during 1988 and 2000), indicating the meteoric origins. Yellow River water and spring water plot near the winter average rainfall, which indicate that they are recharged from the winter rainfall (or snowmelt) or from the area with high elevation. Groundwater displays divergent distribution along the LMWL, indicating various recharge sources with different isotope values. Summer mean rainfall with more enriched $\delta^{2}H$ and $\delta^{18}O$ is isolated from all of the water samples in the YCP, which indicates little summer rainfall recharge under the local meteorological condition.

Figure 6(b) shows that spring water and some of the groundwater lie along the LMWL but do not define the evaporation trend, implying that little evaporation and isotope exchange between groundwater and the rock matrix have occurred. Other groundwater samples locate near the Yellow River water and, moreover, define an evaporation trend (with a slope of 5.5) to the right of the LMWL. The

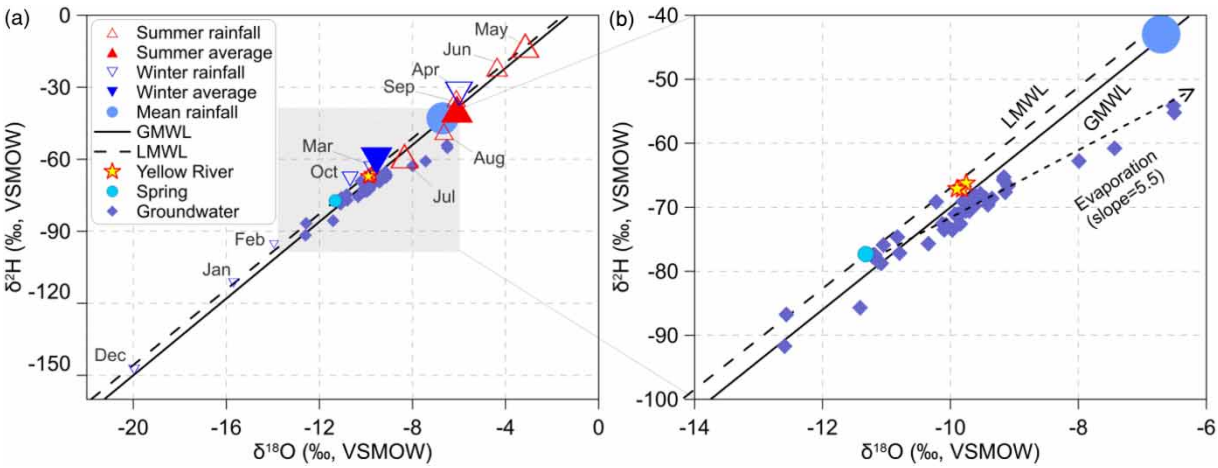

Figure 6 | (a) Plot of stable isotopes for Yellow River water, spring, and groundwater investigated in Yinchuan Plain as compared with the *GMWL* (Craig 1961) and the *LMWL* (rainfall in the Yinchuan station of IAEA networks during 1988 and 2000). 'Mean rainfall' refers to the amount-weighted mean rainfall isotopic value. (b) Shaded region from plot (a).

intersection point of the LMWL and evaporation line is roughly overlapped with the Yellow River water, suggesting the same recharge sources for both the Yellow River water and groundwater. The slope of evaporation line is as low as 5.5 due to the dry air humidity, which is reasonable in the arid areas. Therefore, we can hypothesize that the Yellow River supplies water to the shallow unconfined aquifer in the YCP during which the water molecule fractionate leads to enriched isotope values in the residual groundwater. Irrigation water is being extracted from the Yellow River for the last more than 60 years in the YCP; moreover, precious hydrogeological studies have given a consistent opinion that irrigation water infiltration dominates the shallow unconfined aquifer recharge. As a result of the irrigation infiltration and local rainfall recharge, the groundwater recharge sources might be relatively young and the recharge year could be estimated based on the CFCs.

CFCs were first synthesized in the 1930s, and they can be dissolved in water with various solubilities. The CFC concentrations and ^{3}H activities in groundwater have been widely used to study the young water recharge (post 1940). As can be seen in Tables 1 and 2, groundwater with well depths between 5 and 50 m have detectable CFC concentrations (0.32–4.48 pmol/L for CFC-11, 0.82–2.56 pmol/L for CFC-12, and 0.09–0.38 pmol/L for CFC-113) and ^{3}H activities (3.14–10.48 TU), which evidently indicate the modern water recharge. When old water (pre 1940) is extracted and exposed into the air and then re-infiltrated into the aquifer, confusion arises in the calculation of the groundwater age because the CFCs are water-soluble. Therefore, in this study, we use CFC concentrations to estimate only the recharge year regardless of the groundwater age.

Figure 7 displays the relationship between CFC concentrations and recharge year (calendar year) of groundwater, which is calculated following the method by Plummer *et al.* (2006). The estimated CFC atmospheric partial pressure and recharge year are shown in Table 2.

The collected groundwater recharge year varies from 1964 to 1979 based on CFC-11, from 1974 to 1992 based on CFC-12, and from 1979 to 1988 based on CFC-113. There are some discrepancies among the three CFC-estimated recharge years shown in Figure 7, where the CFC-11-based recharge years are the oldest, while the CFC-12-based and CFC-113-based recharge years are much younger and agree within 4–5 years. We speculate that this phenomenon could be ascribed to some factors as follows. Firstly, despite the groundwater estimate that CFC-based recharge years presuppose the piston flow with no mixing during the groundwater recharge and flow processes, water mixing occurs all the time. The young water (recharge post 1940) mixes in various proportions in the shallow unconfined aquifer. Furthermore, generally there are two water sources for irrigation, one extracted from the Yellow River water and the other from the local groundwater. These two water sources have different CFC concentrations and have different recharge ratios for a shallow unconfined aquifer in the YCP.

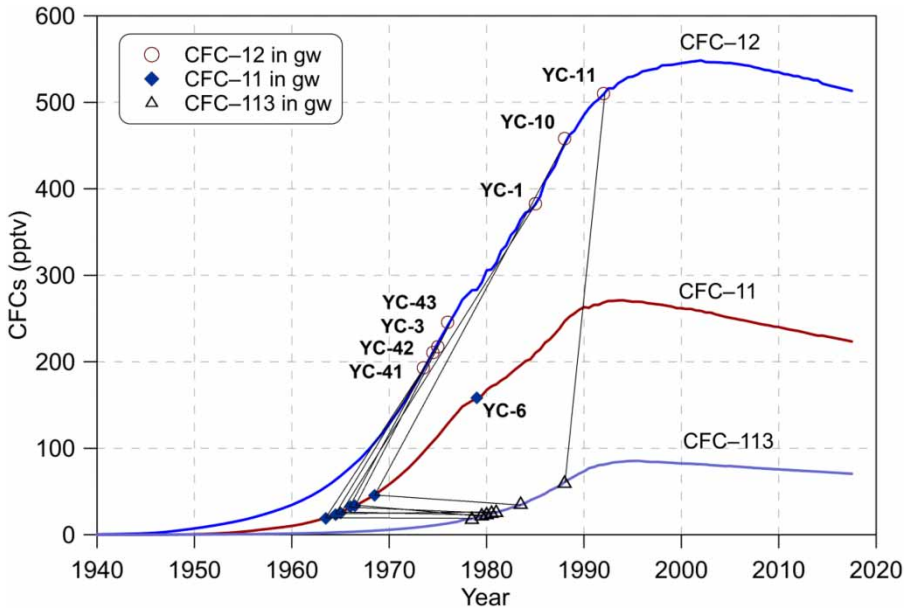

Figure 7 | Concentrations of CFC-11, CFC-12, and CFC-113 (pptv) in the groundwater of this study area sampled in 2019 compared with the time-series trend of the Northern Hemisphere atmospheric mixing ratio.

Secondly, there are time lags for CFC transport through the unsaturated zone (Cook & Solomon 1995), which cause differences in the CFC concentrations. Moreover, the extent of degradation for CFC-11, CFC-12, and CFC-113 varies. Degradation, especially for CFC-11, is common in an anaerobic environment (Plummer *et al.* 2006; Horneman *et al.* 2008), which reduces the CFC-11 concentration in the groundwater and then leads to the relatively old recharge years based on CFC-11. It is unlikely that a groundwater aerobic environment contributes to CFC degradation under anoxic conditions. However, the fine soil textures in the lacustrine plain (Figure 2) lead to a relatively low infiltration process, and, thus, CFC-11 has shown a greater propensity for degradation and/or contamination than CFC-12. Therefore, the CFC-12-based recharge year is discussed in the following text.

It is seen in Figure 7 that No. 10 and 11 groundwater samples have the youngest recharge years, followed by the No.1 groundwater sample. Figure 1 shows that No.10 and 11 groundwater samples are located at the west of Yinchuan and are adjacent to the piedmont plain, where the soil texture consists of pebbles and sandy gravel (Figure 2). No. 1 groundwater locates near the Yellow River southeast of Yinchuan and is far from the piedmont area, which also has a relatively young recharge year. This phenomenon would make us infer that the groundwater lateral flow recharge in the shallow unconfined aquifer is less and that irrigation re-infiltration from the Yellow River water or groundwater plays an important role in the local groundwater recharge. Previous studies that used the water balance method also proved that irrigation infiltration constituted the main recharge source in the YCP.

The inconsistency in the estimation of the recharge years based on CFC-11, CFC-12, and CFC-113 could be attributed to the time-lag effects occurring during water infiltration, which have been verified in other research studies. The time lag for the diffusive transport of CFCs through an unsaturated zone to aquifers is a function of the tracer solubility in water, tracer diffusion coefficients, and soil water content (Cook & Solomon 1995; Qin *et al.* 2011; Darling *et al.* 2012). Figure 7 shows that time lag might be an important factor that influences the groundwater recharge year in the YCP.

Groundwater recharge and mixing characteristics

The atmospheric CFC concentrations vary independently, as seen in Figure 7, which provide us with more information on groundwater recharge and mixing characteristics by comparing CFC-11, CFC-12, and CFC-113 with each other. Firstly, young water (post 1940) recharge and old water (pre 1940) recharge sources can be recognized and

distinguished. Secondly, it helps us to explore quantified data to study the groundwater mixing in which both young water and old (CFC-free) water coexist. Thirdly, the abnormally high CFC concentration indicating urban industrial contamination can be recognized.

As shown in Figure 8(a), groundwater samples can be divided into two groups. No. 3, 41, 42, and 43 groundwater samples locate in the gray-shaded region, suggesting that the recharge sources are comprised by at least various fractions of much younger (post 1980) and older recharge components. The other groundwater samples locate out of the piston flow line, which can be ascribed to CFC-12 contamination or CFC-113 degradation. No. 1, 10, and 11 groundwater samples are in the lower part of the atmospheric CFC concentrations mostly be due to the CFC-113 degradation effect. However, the No. 6 groundwater sample shows an obvious contamination effect for both CFC-12 and CFC-113 concentrations. It is noticed that there is a possibility in Figure 8(a) for some ambiguity around the crossover in the late 1980s, which can result in ambiguous mixing end members when estimating the water mixing ratio. However, in this study, No. 3, 41, 42, and 43 groundwater samples show exclusive binary mixing characteristics, where the end members are CFC-free water (pre-1940 recharge) and young water recharged during the period between 1980 and 1989 (no post-1989 recharge water).

Using the method described by Plummer *et al.* (2006), the binary mixing (Figure 8(a)) results show that the fractions of young water vary from 53.1 to 73.5% (Table 2) for the No. 3, 41, 42, and 43 groundwater samples. Here, we should be wary of the fact that the young water recharge sources could have originated from the precipitation or irrigation re-infiltration from groundwater and Yellow River water.

Furthermore, the cross plot for CFC-12 and CFC-11 (Figure 8(b)) shows that all of the groundwater samples lie off the piston flow curves, which indicates that contamination from the urban air with CFC compounds during sampling or degradation/sorption of CFC-11 has occurred. Nevertheless, previous studies in the arid Northwest China (Barletta *et al.* 2006; Qin 2007) have demonstrated that the urban air with CFC compound contamination in the underdeveloped industrial areas are unlikely. The elevated CFC concentrations, which are much higher than the global background atmospheric CFC concentrations (Northern Hemisphere), have been observed in areas such as Las Vegas, Tucson, Vienna, and Beijing (Barletta *et al.* 2006; Han *et al.* 2007; Qin 2007; Carlson *et al.* 2011). Therefore, in Figure 8, groundwater plotting off the piston flow lines might be ascribed to the sorption effect. Sorption in the unsaturated zone during recharge rather than the CFC degradation under anoxic conditions is more plausible. In addition, No.11 groundwater CFC-11 of No. 11 and CFC-12 of No. 6 are off the piston flow line to

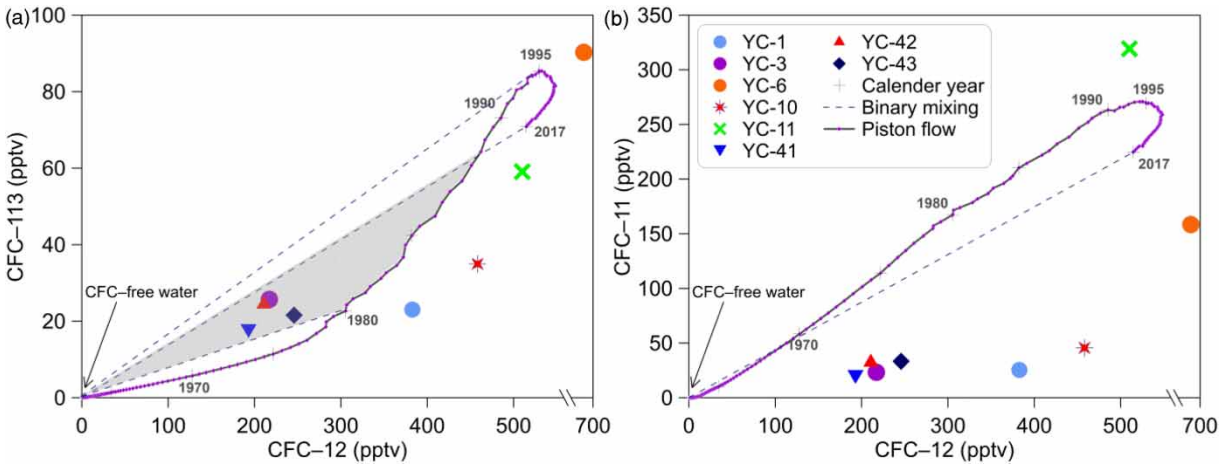

Figure 8 | Plots showing relationships of (a) CFC-113 vs. CFC-12 and (b) CFC-11 vs. CFC-12 in parts per trillion by volume (pptv) for the Northern Hemisphere air. The solid lines correspond to the piston flow and the short-dashed lines show the binary mixing. The '+' denotes the selected calendar year. The shaded regions in (a) indicate no post-1989 water mixing.

much higher concentrations, which likely suggests that contamination of these two groundwater samples has occurred during sampling or measuring.

As a molecule of water, groundwater ^{3}H activity does not vary largely after being exposed in the air, in contrast to CFC concentrations. The combined use of CFCs and ^{3}H may further help to resolve even more complicated mixing scenarios due to the large difference in the temporal pattern of the input functions between CFCs and ^{3}H, such as groundwater mixed with irrigation water and/or young water mixed in different decades.

It is seen in Figure 9 that groundwater No. 1, 3, 41, 42, and 43 plot upward off the piston flow line, which is the same in Figure 8(a) (except for No. 1 sample in Figure 8(a)). Binary mixing can be explained as follows: firstly, these groundwater sources are mixing water recharged in 1989 and between 1940 and 1974, which does not include CFC-free water recharge. Secondly, they are mixing water recharged after 1974. If the second explanation is valid, the binary mixing ratios that are estimated based on CFC-12 and CFC-113 should be the other alternative.

Figure 9 also displays that groundwater No. 6, 10, and 11 have high CFC-12 concentrations but relatively low ^{3}H activities. We can then infer that these water sources are mixed by young water and re-infiltration water (extracted from old groundwater or Yellow River water). Northern hemisphere atmospheric ^{3}H concentrations have been elevated radically since the 1950s, and, thus, old water recharge can be identified by anomalously low ^{3}H activities in comparison with CFCs. Groundwater No. 6 has the lowest ^{3}H activity and the highest CFC-12 concentration, likely indicating that this water sample is extracted from the old groundwater, which, meanwhile, would have been exposed to the air and which finally re-infiltrates into the shallow unconfined aquifer. The low ^{3}H concentration can be ascribed to the dilution by a high fraction of old water, and, thus, the '^{3}H bomb-peak' cannot be recognized. Irrigation re-infiltration can cause a shift in the CFC concentrations to higher values but not alter the ^{3}H concentration (Han *et al.* 2015). Groundwater No. 10 and 11 contain both high CFC-12 concentrations and ^{3}H activities, which could be possible due to mixing with Yellow River water re-infiltration. Irrigation from Yellow River water has been going on unhindered for more than 60 years in the YCP, during which re-infiltration to the shallow unconfined aquifer is possible.

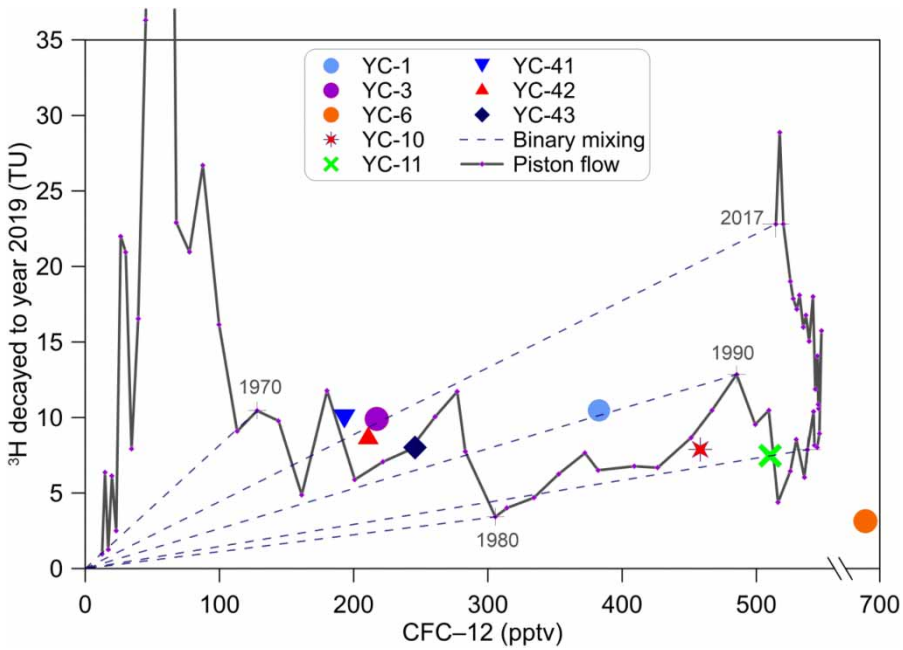

Figure 9 | ^{3}H activity (TU) in Yinchuan precipitation decayed to 2019 vs. CFC-12 (pptv) for Northern Hemisphere air. The solid lines correspond to the piston flow and the short-dashed lines show the binary mixing. The '+' denotes the selected calendar year.

CONCLUSION

In this study, the environmental tracers (^{2}H, ^{18}O, ^{3}H, and CFCs) combining geochemistry with major ions and selected trace elements have enabled us to identify the shallow unconfined aquifer recharge sources and to constrain the young and old water end member mixing rates.

The shallow unconfined aquifer recharge sources are various, including the precipitation recharge in the winter and/or the Helan mountainous precipitation infiltration and then the lateral flow recharge, and the irrigation water re-infiltration abstracted from the local groundwater and the Yellow River. The detailed analysis for groundwater CFC concentrations and ^{3}H activities from the piedmont plain in the Yinchuan west to the lacustrine plain beside the Yellow River suggests that irrigation re-infiltration plays a key role in controlling the shallow unconfined aquifer recharge source. As high as 53.1–73.5% young water ratios have been obtained in the shallow unconfined aquifer in the plain area, where the groundwater mixing characteristics are complicated because of the multiple mixing ratios between young and old water. Regional groundwater geochemical compositions are totally controlled by the groundwater flow pathways form the piedmont plain in the west/south to the lacustrine plain the east/north of the YCP, where evaporite and silicate weathering are the dominant mineral sources. Comparing the shallow and deep aquifer groundwater hydrogeochemical and isotopic data would provide a comprehensive understanding of the regional groundwater flow and recharge. Our CFC data indicated that entrapped excess air has been observed in some shallow groundwater sources, which makes the use of CFCs difficult to study the water cycle. Multiple tracer methods are essential to do further research. To sum up, this study provides quantitative indicators for the shallow unconfined aquifer recharge and mixing characteristics, which is of great practical significance to sustainable water management in the YCP of arid Northwest China.

ACKNOWLEDGMENT

This research was fund by the National Natural Science Foundation of China (No. 41807204).

DATA AVAILABILITY STATEMENT

All relevant data are included in the paper or its Supplementary Information.

REFERENCES

Appelo, C. A. J. & Postma, D. 2005 *Geochemistry, Groundwater and Pollution*, 2nd edn. CRC Press, Balkema, Dordrech, The Netherlands.

Barletta, B., Meinardi, S. & Simpson, I. J. 2006 Ambient halocarbon mixing ratios in 45 Chinese cities. *Atmospheric Environment* **40**, 7706–7719.

Binet, S., Joigneaux, E., Pauwels, H., Albéric, P., Fléhoc, C. & Bruand, A. 2017 Water exchange, mixing and transient storage between a saturated karstic conduit and the surrounding aquifer: groundwater flow modeling and inputs from stable water isotopes. *Journal of Hydrology* **544**, 278–289.

Carlson, M. A., Lohse, K. A., McIntosh, J. C. & McLain, J. E. T. 2011 Impacts of urbanization on groundwater quality and recharge in a semi-arid alluvial basin. *Journal of Hydrology* **409**, 196–211.

Cartwright, I., Weaver, T. R. & Petrides, B. 2007 Controls on $^{87}sr/^{86}sr$ ratios of groundwater in silicate-dominated aquifers: SE Murray Basin, Australia. *Chemical Geology* **246**, 107–123.

Cartwright, I., Cendón, D., Currell, M. & Meredith, K. 2017 A review of radioactive isotopes and other residence time tracers in understanding groundwater recharge: possibilities, challenges, and limitations. *Journal of Hydrology* **555**, 797–811.

Cook, P. G. & Solomon, D. K. 1995 Transport of atmospheric tracer gases to the water table: implications for groundwater dating with chlorofluorocarbons and krypton 85. *Water Resources Research* **31**, 263–270.

Cook, P., Dogramaci, S., McCallum, J. & Hedley, J. 2017 Groundwater age, mixing and flow rates in the vicinity of large open pit mines, Pilbara region, northwestern Australia. *Hydrogeology Journal* **25**, 39–53.

Craig, H. 1961 Isotopic variations in meteoric waters. *Science* **133**, 1702–1703.

Darling, W. G., Gooddy, D. C., MacDonald, A. M. & Morris, B. L. 2012 The practicalities of using CFCs and SF_6 for groundwater dating and tracing. *Applied Geochemistry* **27**, 1688–1697.

Edmunds, W. M., Ma, J. Z., Aeschbach-Hertig, W., Kipfer, R. & Darbyshire, D. P. F. 2006 Groundwater recharge history and hydrogeochemical evolution in the Minqin Basin, North West China. *Applied Geochemistry* **21**, 2148–2170.

Fackrell, J. K., Glenn, C. R., Thomas, D., Whittier, R. & Popp, B. N. 2020 Stable isotopes of precipitation and groundwater provide new insight into groundwater recharge and flow in a structurally complex hydrogeologic system: West Hawai'i, USA. *Hydrogeology Journal* **28**, 1191–1207.

Fan, G. Q. 2018 *The Study of Hydrogen and Oxygen Isotopic and Hydrochemical Characteristics of Water in Yinchuan Plain*. PhD Thesis, Lanzhou University, Lanzhou, China.

Gaillardet, J., Dupré, B., Louvat, P. & Allègre, C. J. 1999 Global silicate weathering and CO_2 consumption rates deduced from the chemistry of large rivers. *Chemical Geology* **159**, 3–30.

Han, L., Hacker, P. & Gröning, M. 2007 Residence times and age distributions of spring waters at the Semmering catchment area, Eastern Austria, as inferred from tritium, CFCs and stable isotopes. *Isotopes in Environmental and Health Studies* **43**, 31–50.

Han, D. M., Song, X. F., Currell, M. J., Cao, G., Zhang, Y. & Kang, Y. 2011 A survey of groundwater levels and hydrogeochemistry in irrigated fields in the Karamay Agricultural Development Area, northwest China: implications for soil and groundwater salinity resulting from surface water transfer for irrigation. *Journal of Hydrology* **405**, 217–234.

Han, D. M., Song, X. F., Currell, M. J. & Tsujimura, M. 2012 Using chlorofluorocarbons (CFCs) and tritium to improve conceptual model of groundwater flow in the South Coast Aquifers of Laizhou Bay, China. *Hydrological Processes* **26**, 3614–3629.

Han, D. M., Cao, G. L., McCallum, J. & Song, X. F. 2015 Residence times of groundwater and nitrate transport in coastal aquifer systems: Daweijia area, northeastern China. *Science of the Total Environment* **538**, 539–554.

Horneman, A., Stute, M., Schlosser, P., Smethie, J. r. W., Santella, N., Ho, D. T., Mailloux, B., Gorman, E., Zheng, Y. & van Geen, A. 2008 Degradation rates of CFC-11, CFC-12 and CFC-113 in anoxic shallow aquifers of Araihazar Bangladesh. *Journal of Contaminant Hydrology* **97**, 27–41.

Huang, T. M. & Pang, Z. H. 2012 The role of deuterium excess in determining the water salinization mechanism: a case study of the arid Tarim River Basin, NW China. *Applied Geochemistry* **27**, 2382–2388.

Huang, T. M., Pang, Z. H., Li, J., Xiang, Y. & Zhao, Z. 2017 Mapping groundwater renewability using age data in the Baiyang alluvial fan, NW China. *Hydrogeology Journal* **25**, 743–755.

Kong, Y. L. & Pang, Z. H. 2016 A positive altitude gradient of isotopes in the precipitation over the Tianshan Mountains: effects of moisture recycling and sub-cloud evaporation. *Journal of Hydrology* **542**, 222–230.

Ma, J. Z., He, J. H., Qi, S., Zhu, G. F., Zhao, W., Edmunds, W. M. & Zhao, Y. P. 2013 Groundwater recharge and evolution in the Dunhuang Basin, northwestern China. *Applied Geochemistry* **28**, 19–31.

Ma, B., Liang, X., Liu, S. H., Jin, M. G., Nimmo, J. R. & Li, J. 2017 Evaluation of diffuse and preferential flow pathways of infiltrated precipitation and irrigation using oxygen and hydrogen isotopes. *Hydrogeology Journal* **25**, 675–688.

Ma, B., Jin, M. G., Liang, X. & Li, J. 2018 Groundwater mixing and mineralization processes in a mountain-oasis-desert basin, northwest China: hydrogeochemistry and environmental tracer indicators. *Hydrogeology Journal* **26**, 233–250.

Ma, B., Jin, M. G., Liang, X. & Li, J. 2019 Application of environmental tracers for investigation of groundwater mean residence time and aquifer recharge in fault-influenced hydraulic drop alluvium aquifers. *Hydrology and Earth System Sciences* **2019** (23), 427–446.

Mahlknecht, J., Hernández-Antonio, A., Eastoe, C. J., Tamez-Meléndez, C., Ledesma-Ruiz, R., Ramos-Leal, J. A. & Ornelas-Soto, N. 2017 Understanding the dynamics and contamination of an urban aquifer system using groundwater age (^{14}C, ^{3}H, CFCs) and chemistry. *Hydrological Processes* **31**, 2365–2380.

Morgenstern, U. & Taylor, C. B. 2009 Ultra low-level tritium measurement using electrolytic enrichment and LSC. *Isotopes in Environmental and Health Studies* **45**, 96–117.

Oster, H., Sonntag, C. & Münnich, K. O. 1996 Groundwater age dating with chlorofluorocarbons. *Water Resources Research* **32**, 2989–3002.

Parkhurst, D. L. & Appelo, C. A. J. 1999 User's guide to PHREEQC (Version 2): a computer program for speciation, batch-reaction, one-dimensional transport, and inverse geochemical calculations. US Geological Survey. *Water Resource Investigations Report* 99–4259.

Plummer, L. N., Busenberg, E. & Cook, P. G. 2006 In: *Use of Chlorofluorocarbons in Hydrology: A Guidebook* (M. Gröning, L. F. Han & P. Aggarwal, eds). International Atomic Energy Agency, Vienna, Austria.

Qin, D. J. 2007 Decline in the concentrations of chlorofluorocarbons (CFC-11, CFC-12 and CFC-113) in an urban area of Beijing, China. *Atmospheric Environment* **41**, 8424–8430.

Qin, D. J., Qian, Y. & Han, L. 2011 Assessing impact of irrigation water on groundwater recharge and quality in arid environment using CFCs, tritium and stable isotopes, in the Zhangye Basin, Northwest China. *Journal of Hydrology* **405**, 194–208.

Stallard, R. F. & Edmond, J. M. 1987 Geochemistry of the Amazon: weathering chemistry and limits to dissolved inputs. *Journal of Geophysical Research* **92**, 8293–8302.

Su, X. S. & Lin, X. Y. 2004 Cycle pattern and renewability evaluation of groundwater in Yinchuan Basin: Isotopic evidences. *Resources Science* **26**, 29–35.

Tadros, C. V., Hughes, C. E., Crawford, J., Hollins, S. E. & Chisari, R. 2014 Tritium in Australian precipitation: a 50 year record. *Journal of Hydrology* **513**, 262–273.

Wang, W. K., Han, J. P., Zhao, Y. Q., Yu, D. M. & Wang, H. Y. 2004 Optimal allocation of water resources in Yinchuan Plain. *Resources Science* **26**, 36–45.

Yang, Q. C. 2018 *Hydrochemical Formation Mechanism and Water Quality Analysis of Phreatic Water in Yinchuan Plain Under the Influences of Anthropogenic Activities*. PhD thesis, Jilin University, Jilin, China.

Zhu, G. F., Li, Z. Z., Su, Y. H., Ma, J. Z. & Zhang, Y. Y. 2007 Hydrogeochemical and isotope evidence of groundwater evolution and recharge in Minqin Basin, Northwest China. *Journal of Hydrology* **333**, 239–251.

First received 3 October 2020; accepted in revised form 9 March 2021. Available online 22 March 2021